Simulations of Solar Wind Charge Exchange X-ray emissions at Venus

H. Gunell[1]

Department of Physics, West Virginia University, Morgantown, WV 26506-6315

E. Kallio, R. Jarvinen, and P. Janhunen

Finnish Meteorological Institute, Helsinki, Finland

M. Holmström

Swedish Institute of Space Physics, Kiruna, Sweden

K. Dennerl

Max-Planck-Institut für extraterrestrische Physik, Garching, Germany

A hybrid simulation of the solar wind-Venus interaction and a test particle simulation of heavy ion trajectories near Venus are used to compute the contribution from solar wind charge exchange processes to the X-ray emission from Venus. It is found that the X-ray halo caused by the solar wind charge exchange process at Venus is confined to lower altitudes than at Mars, and that the structure on the ion gyro radius scale that is seen in X-ray images of Mars is absent at Venus.

1. Introduction

X-rays are emitted through the solar wind charge exchange process wherever the solar wind meets a neutral atmosphere. A small fraction of the solar wind consists of highly charged ions such as O^{6+}, C^{6+}, and Ne^{8+}. Charge-exchange collisions between these ions and neutral atoms can leave the ions in highly excited states. These highly excited ions then undergo transitions to lower energy states, emitting photons in the soft X-ray range. *Cravens* [1997] first proposed this process as an explanation for the observations of X-rays from comets, and it is likely the dominant process for generation of cometary X-rays [*Cravens*, 2002]. Solar wind charge exchange has also been suggested as a mechanism for generation of X-rays at Mars [*Cravens*, 2000; *Krasnopolsky*, 2000]. Computer simulations of the intensities and morphology of these emissions were presented by *Holmström et al.* [2001] for Mars.

Fluorescence is another X-ray generating process that is active at planets. It occurs when X-rays emitted by the sun are absorbed by neutrals in the planetary atmosphere, and then re-emitted isotropically. Elastic scattering of solar X-rays can also occur in planetary atmospheres. A detailed analysis of the intensity of the X-rays produced by these two mechanisms was done by *Cravens and Maurellis* [2001].

In recent years the unmagnetised planets, Venus and Mars, have been observed in X-rays. A disk the size of Mars dominated by fluorescent scattering of solar X-rays was found when Mars was observed by the Chandra X-ray observatory in the year 2001 [*Dennerl*, 2002]. Around the disk a faint X-ray halo was detected. It could not be explained by fluorescence, since the fluorescence peak, that is seen in the emissions from the disk, is absent in the X-ray emissions from the halo [*Dennerl*, 2002], and fluorescence is an efficient process only at low altitudes. *Dennerl* [2002] suggested that the halo could be caused by the solar wind charge exchange process. *Gunell et al.* [2004] performed a computer simulation that showed that charge exchange processes are consistent with the observations of the Martian X-ray halo. The sensitivity to changes in the parameters was investigated by *Gunell et al.* [2005b]. When Mars was observed using the XMM-Newton X-ray telescope a more detailed X-ray spectrum was obtained, and soft X-ray line emissions from highly charged ions could be identified in the halo [*Dennerl et al.*, 2006]. It could thus be confirmed that the halo is caused by the solar wind charge exchange process.

Venus was observed in X-rays using the Chandra X-ray observatory in 2002 [*Dennerl et al.*, 2002]. It appeared as a half-lit crescent, with considerable brightening on the sunward limb. This morphology, as well as the spectrum and luminosity, agreed with fluorescent scattering of solar X-rays. In contrast to Mars, no indications for an extended X-ray halo were found. Venus was observed again on the 27th and 28th of March 2006, with an increased sensitivity, but the analysis of that observation has not yet been completed.

In this paper we present new simulation results of the charge exchange X-ray emissions at Venus, and compare these to the previous results from Mars.

2. Simulation model

The simulations were performed in two steps. First we ran a quasi-neutral hybrid model of the interaction between Venus and the solar wind [*Kallio et al.*, 2006]. In the hybrid model the ions are treated as particles, the motion of which are governed by the Lorentz force. The electrons are treated as a massless charge neutralising fluid. The hybrid model produced values of the electric and magnetic fields on a grid around Venus. Secondly we performed a test particle simulation for a number of the most important highly charged ion species in the solar wind. With knowledge of the particle trajectories; the neutral exosphere density; the charge exchange cross sections; and the transition probabilities, the X-ray emissions can be calculated. The test particle simulation and the image generation is performed using the

[1]Previously at the Swedish Institute of Space Physics, Kiruna, Sweden

same algorithms that were previously used for the calculation of the charge exchange X-rays from Mars [*Gunell et al.*, 2004, 2005b].

The input parameters to the hybrid simulation were the same as those used by *Kallio et al.* [2006]. These are summarised in table 1, where u_{sw} is the bulk velocity of the solar wind, n_{sw} the proton density of the solar wind, T_p the solar wind proton temperature, and $\vec{B}$ the solar wind magnetic flux density.

The coordinate system that is used here has its origin at the centre of Venus. The x-axis points from Venus towards the Sun. The z-axis is defined by $\vec{u}_z = (\vec{v} \times \vec{u}_x)/|\vec{v} \times \vec{u}_x|$, where $\vec{u}_x$ is a unit vector in the positive x-direction, and $\vec{v}$ is the velocity of Venus in its orbit around the Sun, i.e., z is perpendicular to the orbital plane of Venus. The y-axis completes the right-handed coordinate system. The simulation was run until $t = 240$ s, and then the electric and magnetic fields were saved.

The second step was to run a test particle simulation, calculating the trajectories of highly charged solar wind ions in the electric and magnetic fields that were obtained from the hybrid simulation, and for each time step of the test particle simulation saving the X-ray production rate on a grid. One hundred thousand trajectories were calculated for each of the ion species O^{7+}, C^{6+}, O^{6+}, O^{8+}, Mg^{10+}, Mg^{9+}, Si^{9+}, N^{6+}, C^{5+}, Ne^{8+}, Fe^{9+}, S^{9+}, Si^{8+}, Fe^{11+}, and Mg^{8+}. These species were selected from table 1 of *Schwadron and Cravens* [2000] for being the ion species that generate the highest luminosity, and together comprising 91.6 % of the total luminosity of the species in that table. The charge exchange cross sections were taken from the same table. The test particles were injected into the simulation box upstream from Venus with the bulk and thermal speeds that are given in table 1. All species are assumed to have the same thermal speed, which is usually the case in the solar wind [*Hefti et al.*, 1998]. The relative abundances for the different ion species were taken from *Schwadron and Cravens* [2000]. The same neutral exosphere model is used in the hybrid simulations and in the test particle simulations. It includes hot and cold populations of atomic hydrogen and a hot atomic oxygen component, and it was described in detail by *Kallio et al.* [2006]. A similar model was previously used to study generation of energetic neutral atoms at Venus [*Gunell et al.*, 2005a].

3. Venus calculation results

Fig. 1 shows the positions of the sun, the earth, and Venus at 15:30 UT on 27 March 2006. This was the configuration of the planets when Venus was observed in X-rays by the Chandra X-ray observatory.

Table 1. Solar wind parameters used in the quasi-neutral hybrid simulation.

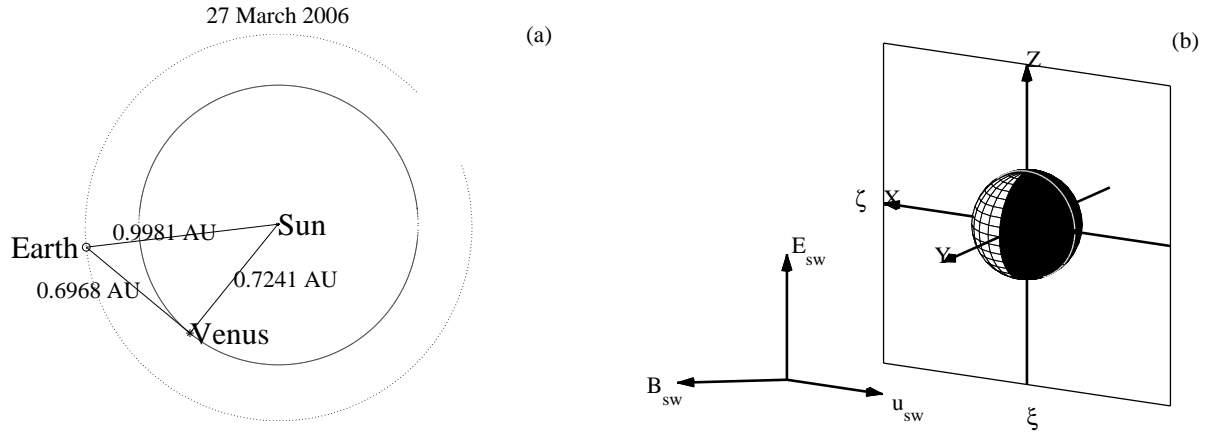|	
$\vec{u}_{sw}$	$(-430, 0, 0)$ km/s
n_{sw}	$1.4 \times 10^7 \mathrm{m}^{-3}$
$v_{th} = \sqrt{k_B T_p/m_p}$	50 km/s
$\vec{B}$	$(8.09, 5.88, 0)$nT $=$ 10nT $\cdot (\cos(36°), \sin(36°), 0)$

Figure 1. (a) The position of Earth and Venus at 15:30 UT on 27 March 2006. This was the configuration of the planets when Venus was observed in X-rays by the Chandra X-ray observatory on 27–28 March 2006. (b) The planetary coordinates x, y, and z, and the image coordinates ξ and ζ. The directions of the solar wind velocity u_{sw}, its magnetic field B_{sw}, and convective electric field E_{sw} are also shown.
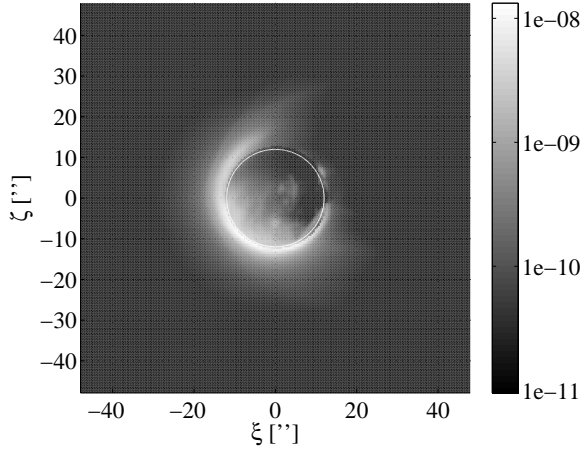
Figure 2. A simulated X-ray image of Venus as seen from an observer at the earth assuming the planetary configuration shown in Fig. 1. The grey-scale shows the X-ray radiance in $Wm^{-2}sr^{-1}$. The coordinates ξ and ζ are shown in arc seconds as seen by an observer at the earth.
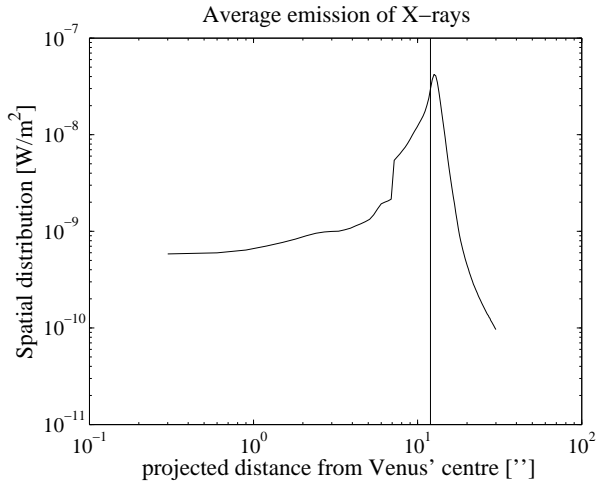

Figure 3. Radial distribution of X-ray emissions. The curve shows the result of integrating the image in Fig. 2 over the azimuthal angle.

Fig. 2 shows a simulated image of the solar wind charge exchange X-rays emitted from Venus as seen from an observer at the earth assuming the planetary configuration shown in Fig. 1. Since the phase angle is 89.2°, which is very close to 90°, the sun is almost exactly in the image plane, to the left of the image itself. The image coordinates are further explained in Fig. 1(b). The X-ray emissions are concentrated to low altitudes, and occur mostly on the dayside, but reach into the nightside in the southern hemisphere. There is

a clear asymmetry between the northern and southern hemispheres with stronger and lower altitude emissions in the south and weaker emissions at higher altitudes in the north. This asymmetry is caused by the shocked solar wind flow reaching lower altitudes in the southern than in the northern hemisphere [*Kallio et al.*, 2006]. The asymmetry in the flow is an effect of the solar wind magnetic field. The solar wind convective electric field is directed upward in the figure, as is also shown in Fig. 1(b). Due to the sharp falloff of the neutral density with altitude the X-ray emissions are very sensitive to changes in the altitude of the plasma ion flow.

The test particle simulations were performed using the electric and magnetic fields in the hybrid simulation at one instant in time. If the solar wind conditions change during an observation period of 22 hours features seen in a simulation corresponding to the conditions at one instant in time may be averaged away.

Fig. 3 shows the radial distribution of the simulated X-ray power, i.e., Fig. 3 is Fig. 2 integrated over the azimuthal angle. The vertical line at 12.1" in Fig. 3 shows the angular size of Venus. The emissions peak at a low altitude, corresponding to 12.6", and fall off two orders of magnitude within eight arc seconds. This sets the requirements on the spatial resolution needed for detection of the X-ray halo at Venus.

4. Mars–Venus comparison

Fig. 4 shows simulated X-ray images from Venus (left panel) and Mars (right panel). The vantage points have been chosen such that the radius of each planets subtends an angle of exactly ten arc seconds. In both cases the sun is in the image plane to the left of the image. For Venus this is close to the situation during the observation on 27 March 2006, whereas for Mars it corresponds to a vantage point that is located outside Mars orbit and therefore not accessible to Earth-orbiting telescopes.

The X-ray image of Mars in Fig. 4 was calculated using the same hybrid and test particle simulation results as those used by *Gunell et al.* [2004]. Only the vantage point differs from what was used to generate the previously published images of Mars.

The mass of Venus is 7.5 times that of Mars and therefore the exosphere density falls off faster with altitude at Venus than it does at Mars. Thus the extent of the Mars' exosphere is greater than the extent of Venus' exosphere, and this is reflected also in the charge exchange X-ray images, that show a more extended emission region at Mars than at Venus. At Venus the emissions are confined to low altitudes. The grey scale is the same in the two images and thus the peak emissions are comparable in magnitude.

The filamentary structure, the width of which is on the ion gyro radius size scale, that is seen in the im-
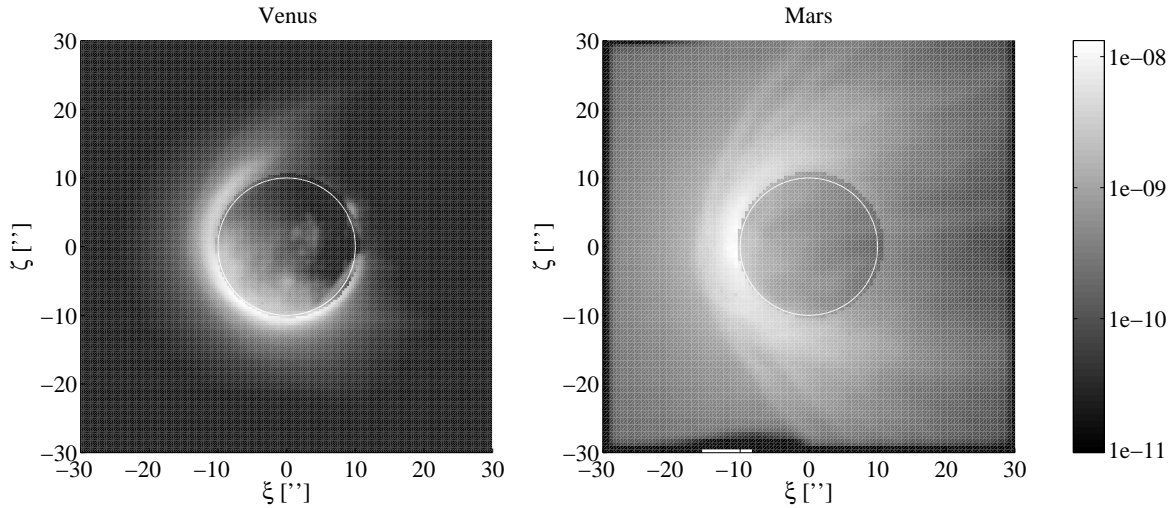
Figure 4. Simulated X-ray Images of Venus and Mars. The vantage points are chosen such that the angular size is the same for the two planets. One planetary radius subtends ten arc seconds. The sun is in the image plane to the left of the image. The grey-scale shows the X-ray radiance in $Wm^{-2}sr^{-1}$. The white circles mark the geometric size of the respective planets.

age of Mars, is absent at Venus. Due to the stronger magnetic field and larger planet size at Venus the gyro radius to planetary radius ratio is smaller at Venus than at Mars. Also at the altitude where this structure appears at Mars the Venus exosphere density has already dropped to very low values.

A north-south asymmetry is seen in the image of Venus. This is a result of the solar wind magnetic field causing the shocked solar wind flow to reach lower altitudes in the southern than in the northern hemisphere [*Kallio et al.*, 2006]. This asymmetry is far less pronounced at Mars than at Venus, although it can be noticed if the image of Mars in Fig. 4 is examined carefully. At both planets the magnetic and electric fields are asymmetric near the planet due to finite Larmor radius effects. The X-ray emissions are more asymmetric at Venus than at Mars, because the plasma encounters high neutral densities near the planet only in case of Venus.

5. Conclusions

We have presented simulated charge exchange X-ray images of Venus. The images were computed using a two step process, where first a quasi-neutral hybrid code was run to compute the electric and magnetic fields around Venus. Secondly, the X-ray emissions were calculated using a test particle simulation for a number of highly charged solar wind ion species.

The image in Fig. 2 was computed using the geometrical situation at the time when Venus was observed by Chandra in March 2006. It shows a pronounced brightening at the limb, plus some brightening in front of the disk. Our simulation results will be compared to the ob-

servational results in a future paper, when the analysis of data obtained by Chandra is complete.

Since the solar wind parameters for Venus at that time are unknown we have used standard solar wind parameters that were previously used by *Kallio et al.* [2006]. In addition to this source of error the calculations are subject to the same uncertainties as our earlier calculations of X-rays from Mars: The exosphere densities; solar wind ion abundances; charge exchange cross sections; and the hybrid code electric and magnetic field results are all potential sources of error.

The test particle simulations were performed using the electric and magnetic fields in the hybrid simulation at one instant in time. In reality the solar wind parameters and hence the fields will vary during 22 hours of observation. A consequence of this can be that features that are seen in the simulation will be averaged away in the observation. Although there are fluctuations in the simulation during the course of its run, the important contribution to this effect is the temporal variations in the solar wind. So far there is no X-ray observation of Venus with simultaneous measurements of the solar wind parameters. When such an observation occurs it will be possible to better model the observations by running several simulations for a set of different parameters, and subsequently form a weighted average of the results. Simultaneous X-ray and plasma measurements at Venus are planned for 6 June 2007 when the Messenger spacecraft flies by Venus, and the Venus Express spacecraft still will be in orbit around the planet.

The exosphere at Venus falls off more rapidly with altitude than the Martian exosphere. This makes the altitude range where the neutral density is high enough to produce X-rays of any intensity more narrow at Venus.

The maximum intensity in the charge exchange X-ray image of Venus is comparable to the maximum intensity in the corresponding image of Mars. However, the emissions at Venus are concentrated to lower altitude and the intensity falls two orders of magnitude within eight arc seconds, which means that the spatial resolution requirements for detection of the charge exchange X-ray halo at Venus are more severe. Instead of geometrically identifying a halo the spectral information could be used to distinguish fluorescent X-rays from charge exchange X-rays.

The structure on the size of the ion gyro radius that is seen at Mars is absent at Venus.

6. Acknowledgements

References

Cravens, T. E., Comet Hyakutake x-ray source: Charge transfer and solar wind heavy ions, *Geophys. Res. Lett.*, *24*, 105–108, 1997.

Cravens, T. E., X-ray emission from comets and planets, *Adv. Space Res.*, *26*(10), 1443–1451, 2000.

Cravens, T. E., X-ray emission from comets, *Science*, *296*, 1042–1045, 2002.

Cravens, T. E., and A. N. Maurellis, X-ray emission from scattering and fluorescence of solar x-rays at venus and mars, *Geophys. Res. Lett.*, *28*(15), 3043–3046, 2001.

Dennerl, K., Discovery of X-rays from Mars with Chandra, *Astronomy & Astrophysics*, *394*, 1119–1128, doi:10.1051/0004-6361:20021116, 2002.

Dennerl, K., V. Burwitz, J. Englhauser, C. Lisse, and S. Wolk, Discovery of X-rays from Venus with Chandra, *Astronomy & Astrophysics*, *386*, 319–330, doi:10.1051/0004-6361:20020097, 2002.

Dennerl, K., et al., Mars observed with XMM-Newton: High resolution X-ray spectroscopy with RGS, *Astronomy & Astrophysics*, *451*, 709–722, doi:10.1051/0004-6361:20054253, 2006.

Gunell, H., M. Holmström, E. Kallio, P. Janhunen, and K. Dennerl, X-rays from solar wind charge exchange at Mars: A comparison of simulations and observations, *Geophys. Res. Lett.*, *31*, L22801, doi:10.1029/2004GL020953, 2004.

Gunell, H., M. Holmström, H. K. Biernat, and N. V. Erkaev, Planetary ENA imaging: Venus and a comparison with mars, *Planetary and Space Science*, *53*(4), 433–441, doi:10.1016/j.pss.2004.07.021, 2005a.

Gunell, H., M. Holmström, E. Kallio, P. Janhunen, and K. Dennerl, Simulations of X-rays from solar wind charge exchange at Mars: Parameter dependence, *Adv. Space Res.*, doi:10.1016/j.asr.2005.06.007, 2005b.

Hefti, S., et al., Kinetic properties of solar wind minor ions and protons measured with SOHO/CELIAS, *J. Geophys. Res.*, *103*(A12), 29,697–29,704, 1998.

Holmström, M., S. Barabash, and E. Kallio, X-ray imaging of the solar wind–Mars interaction, *Geophys. Res. Lett.*, *28*(7), 1287–1290, 2001.

Kallio, E., R. Jarvinen, and P. Janhunen, Venus-solar wind interaction: Asymmetries and the escape of O^+ ions, *Planetary and Space Science*, *54*, 1472–1481, doi:10.1016/j.pss.2006.04.030, 2006.

Krasnopolsky, V., On the deuterium abundance on Mars and some related problems, *Icarus*, *148*, 597–602, 2000.

Schwadron, N. A., and T. E. Cravens, Implications of solar wind composition for cometary X-rays, *The Astrophysical Journal*, *544*, 558–566, 2000.

H. Gunell, Department of Physics, West Virginia University, Morgantown, WV 26506-6315 (herbert.gunell@physics.org)

E. Kallio, Finnish Meteorological Institute, Space Research, P.O. Box 503, FIN-00101 Helsinki, Finland (esa.kallio@fmi.fi)

R. Jarvinen, Finnish Meteorological Institute, Space Research, P.O. Box 503, FIN-00101 Helsinki, Finland (riku.jarvinen@fmi.fi)

P. Janhunen, Finnish Meteorological Institute, Space Research, P.O. Box 503, FIN-00101 Helsinki, Finland (pekka.janhunen@fmi.fi)

M. Holmström, Swedish Institute of Space Physics, Box 812, SE-981 28 Kiruna, Sweden (matsh@irf.se)

K. Dennerl, Max-Planck-Institut für extraterrestrische Physik, Giessenbachstraße, 85748 Garching, Germany (kod@mpe.mpg.de)